

N 型低溫多晶矽薄膜電晶體元件特性及 可靠度之統計性研究

研究生:周彥邦

指導教授:戴亞翔 博士

國立交通大學

光電工程學系光電工程研究所



摘要

多晶矽薄膜電晶體(poly-Si TFTs)基於其優於非晶矽薄膜電晶體(amorphous silicon TFTs)的電流驅動能力，最近在液晶顯示器(AMLCD)及有機發光二極體(AMOLED)顯示器的週邊電路整合應用上皆備受矚目。在本文中，我們將對低溫多晶矽薄膜電晶體(low temperature poly-Si TFTs)的元件特性作一統計性的研究。對於在固定距離下兩元件間特性如臨界電壓(threshold voltage)及遷移率(mobility)之差異，會做進一步的討論。這些元件間差異行為的變異性(variation)分布將可以用我們所提出的數學模型加以描述，取代之之前所廣泛採用的高斯分布。而在這些我們所提出函數對於實際量測到的分布之比較中，經過回歸分析所得之回歸變異係數(R square)皆在 0.95 之上。此一結果代表我們所提出的變異性的模型與實際分布情況十分吻合，也反映出該模型的適用性。更進一步的，本文所提出的模型會用於在面板週邊驅動電路中常用到的差動對(differential pair)之模擬。我們將可以從模擬的結果之中，了解電路上元件間的變異性對電路性能產

生之影響。

論文的最後會對元件的可靠度以各種不同的偏壓條件及偏壓時間來衡量。我們將以本文所提出之枕木型佈局的電晶體作可靠度的量測以避免元件間初始特性差異過大，導致在同一偏壓條件下得到發散的結果。經由這些實驗資料將會對估計元件的生命週期和安全的操作區域將是十分有幫助的。




Statistical Study on the Characteristics and Reliability Behaviors of N-type LTPS TFTs

Student : Yen-Pang Chou

Advisor : Dr.Ya-Hsiang Tai

Department of Photonics & Institute of Electro-optical Engineering,
National Chiao Tung University

Abstract

The logo of National Chiao Tung University is a circular emblem. It features a gear-like outer border. Inside the circle, there is a stylized representation of a building or a ship, and the year '1896' is inscribed at the bottom of the inner circle.

Low Temperature Polycrystalline Silicon (LTPS) thin film transistors (TFTs) have attracted much attention in the application on the integrated peripheral circuits of display electronics such as active matrix liquid crystal displays (AMLCDs) and active matrix organic light emitting diodes (AMOLEDs) due to its better current driving compared with a-Si (amorphous silicon) TFTs. In this thesis, the variation characteristics of LTPS TFTs are statistically investigated. The differences of the threshold voltage and mobility with the same device distance are further studied. The difference shows the distribution much centered than the Gaussian distribution and a proper model is proposed to describe the variation behaviors with difference device distances, for which the R squares (Coefficient of Determination) are higher than 0.95, reflecting the validity of the model. Furthermore, the proposed models are used to simulate the performance of the differential pair, which is commonly used in driving of the panel. Simulation results show the effects of the variation behavior on the estimation of the circuit performance.

Finally, the reliability of LTPS TFTs is studied in form of stress map by adopting the crossie layout TFTs to get the more consistent reliability behaviors. This database of reliability is very helpful to evaluate the lifetime and operation conditions of LTPS TFTs.



誌 謝

在短短的兩年研究所生活中，很幸運的能擁有非常良好的研究環境來完成碩士班的訓練。首先要感謝的是我的指導教授戴亞翔老師。在老師的言教及身教引導下，不僅使我在研究上能有所成果並且從中獲得啟發；在待人處世方面，更是獲益良多，也使我能從軍旅生涯中順利的過渡到研究所的生活。在此要向戴老師致上最誠摯的敬意及謝意。

除此之外，很感謝士哲學長在我的研究方向及專業領域的指導，婉萍在統計學上的協助。還有之前畢業學長和實驗室學弟妹，以及隔壁實驗室的同學們；你們不管在研究上、生活上，都提供了我莫大的幫助，陪著我共同度過這段研究的時光。

最後要感謝的是我的父母及家人，和我周遭的朋友們。你們一直是我精神上最大的支柱，讓我能無後顧之憂的致力於研究工作；最後，謹以此論文獻給你們。

彥邦 2006.01

Contents

Chinese Abstract	I
English Abstract	III
Acknowledgement	V
Contents	VI
Figure Captions	VIII

Chapter 1. Introduction

1-1. Introduction to LTPS TFTs	1
1-2. Diverse reliability behaviors	2
1-3. Device variation	2
1-4. Motivation	3
1-5. Thesis outline	4

Chapter 2. Statistical analysis of crosstie TFT device parameters

2-1. Introduction to crosstie TFTs	6
2-2. Device fabrication and parameter extraction	7
2-2-1. Device fabrication	7
2-2-2. Parameter extraction	7
2-3. Initial parameter distribution	9
2-4. The difference of initial parameter distribution	10
2-4-1. The distribution with different device distance	10
2-4-2. The models of distributions	11

Chapter 3. Effects of device distribution on circuit performance

3-1. Introduction to the differential pair	14
3-2. Evaluation of the circuit performance with proposed models and other	

simulation skills	15
3-3. Discussion and conclusion	19
Chapter 4. Stress mapping for reliability	
4-1. Motivation	21
4-2. Experiment and degradation mechanism	21
4-2-1. Setup for the stress map	21
4-2-2. Degradation mechanism	22
4-3. Results and discussion	23
Chapter 5. Conclusion	26
References	28
Figures	30
Vita	64



Figures Captions

Chapter 1

Fig. 1-1 The block diagram of an active matrix display

Fig. 1-2 The integration of peripheral circuits in a display achieved by poly-Si TFTs

Fig. 1-3 The variation of threshold voltage shift under different stress conditions

Fig. 1-4 The variation of mobility degradation under different stress conditions

Fig. 1-5 The initial characteristics of LTPS TFTs are different from one another due to various distributions of grain boundaries

Fig. 1-6 The site variation of the threshold voltage variation for LTPS TFT fabrication line plotted in the format of lot trend

Chapter 2

Fig. 2-1 The layout of the crosstie TFTs

Fig. 2-2 The schematic cross-section structure of the n-type poly-Si TFT with lightly doped drain

Fig. 2-3 The distributions of threshold voltage for crosstie TFTs

Fig. 2-4 The distributions of mobility for crosstie TFTs

Fig. 2-5 The distributions of subthreshold for crosstie TFTs

Fig. 2-6 The grain boundary number in the channel length direction

Fig. 2-7 The distributions of initial parameters vary with the different sites on glass and lot

Fig. 2-8 The average and the standard deviation of the differences of threshold voltage

Fig. 2-9 The average and the standard deviation of the differences of mobility

Fig. 2-10 The average and the standard deviation of the differences of subthreshold swing

Fig. 2-11 The threshold voltage distribution along the device position

Fig. 2-12 Simulation of the threshold voltage distribution along the device position for a long range

Fig. 2-13 (a) The distribution of V_{th} deference and its fitting curve under the device distance of $40 \mu\text{m}$

Fig. 2-13 (b) The distribution of V_{th} deference and its fitting curve under the device distance of $200 \mu\text{m}$

Fig. 2-13 (c) The distribution of V_{th} deference and its fitting curve under the device distance of $2000 \mu\text{m}$

Fig. 2-13 (d) The distribution of V_{th} deference and its fitting curve under the device distance of $4000 \mu\text{m}$

Fig. 2-13 (e) The distribution of V_{th} deference and its fitting curve under the device distance of $8000 \mu\text{m}$

Fig. 2-13 (f) The distribution of V_{th} deference and its fitting curve under the device distance of $12000 \mu\text{m}$

Fig. 2-14 (a) The distribution of mobility deference and its fitting curve under the device distance of $40 \mu\text{m}$

Fig. 2-14 (b) The distribution of mobility deference and its fitting curve under the device distance of $200 \mu\text{m}$

Fig. 2-14 (c) The distribution of mobility deference and its fitting curve under the device distance of $2000 \mu\text{m}$

Fig. 2-14 (d) The distribution of mobility deference and its fitting curve under the device distance of $4000 \mu\text{m}$

Fig. 2-14 (e) The distribution of mobility deference and its fitting curve under the device distance of $8000 \mu\text{m}$

Fig. 2-14 (f) The distribution of mobility deference and its fitting curve under the device distance of $12000 \mu\text{m}$

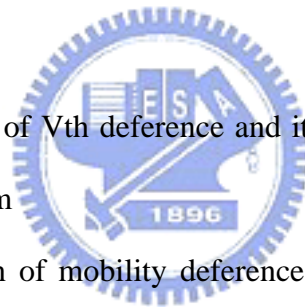


Fig. 2-15 (a) The distribution of S.S deference and its fitting curve under the device distance of 40 μm

Fig. 2-15 (b) The distribution of S.S deference and its fitting curve under the device distance of 200 μm

Fig. 2-15 (c) The distribution of S.S deference and its fitting curve under the device distance of 2000 μm

Fig. 2-15 (d) The distribution of S.S deference and its fitting curve under the device distance of 4000 μm

Fig. 2-15 (e) The distribution of S.S deference and its fitting curve under the device distance of 8000 μm

Fig. 2-15 (f) The distribution of S.S deference and its fitting curve under the device distance of 12000 μm

Fig. 2-16 (a) The fitting parameters, a and d of V_{th} difference versus the device distance

Fig. 2-16 (b) The fitting parameters, b and c of V_{th} difference versus the device distance

Fig. 2-17 The fitting parameters of Mu difference versus the device distance

Fig. 2-18 The fitting parameters of Mu difference versus the device distance

Chapter 3

Fig. 3-1 (a) The coupling effects of the clock signal

Fig. 3-1 (b) The signal transmission is done by differential signal

Fig. 3-2 Basic differential pair structure

Fig. 3-3 The equivalent for common mode operation

Fig. 3-4 (a) The equivalent for common mode operation (V_{in1} on, V_{in2} off)

Fig. 3-4 (b) The equivalent for common mode operation (V_{in1} off, V_{in2} on)

Fig. 3-5 Simple distribution with four variables

Fig. 3-6 The chart for data transformation

Fig. 3-7 The simulation results for CMRR value with different models

Chapter 4

Fig. 4-1 Four regions of stress mapping and the gray circles are the stress conditions for the test

Fig. 4-2 (a) The degradation behaviors of V_{th} under the stress time of 10 sec

Fig. 4-2 (b) The degradation behaviors of V_{th} under the stress time of 50 sec

Fig. 4-2 (c) The degradation behaviors of V_{th} under the stress time of 100 sec

Fig. 4-2 (d) The degradation behaviors of V_{th} under the stress time of 1000 sec

Fig. 4-3 (a) The degradation behaviors of mobility under the stress time of 10 sec

Fig. 4-3 (b) The degradation behaviors of mobility under the stress time of 50 sec

Fig. 4-3 (c) The degradation behaviors of mobility under the stress time of 100 sec

Fig. 4-3 (d) The degradation behaviors of mobility under the stress time of 1000 sec

Fig. 4-4 (a) The degradation behaviors of S.S under the stress time of 10 sec

Fig. 4-4 (b) The degradation behaviors of S.S under the stress time of 50 sec

Fig. 4-4 (c) The degradation behaviors of S.S under the stress time of 100 sec

Fig. 4-4 (d) The degradation behaviors of S.S under the stress time of 1000 sec